AD-A256 764

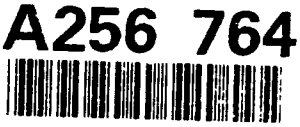

(12)

CR 92.009

NCEL

Contract Report

August 1992

An Investigation Conducted by
Gregg L. Fiegel and Bruce L. Kutter
University of California, Davis

DTIC
ELECTE
OCT 15 1992
S B D

THE MECHANISM OF LIQUEFACTION IN LAYERED SOILS

Abstract Results from six centrifuge model tests are presented. Four of the model tests involve layered soil deposits subject to base shaking; two model tests involve uniform soil deposits of sand subject to base shaking. The layered soil models consisted of a saturated liquefiable fine sand overlain by a layer of relatively impermeable silica flour (silt). Pore water pressures, accelerations, and settlements were measured during all six tests. Results from the model tests involving layered soils suggest that during liquefaction, a water interlayer or very loose zone of soil develops between the sand and the silt due to the difference in permeabilities. Soil volcanos or boils were seen on the surface for all four of these layered model tests. The locations of these boils, in each test, were found concentrated in the weakest zones of the overlying silt layer; cracking of the weak silt zones provided a release or a vent for the excess e water pressure generated as a result of particle rearrangement in the liquefiable fine sand.

92-27077

NAVAL CIVIL ENGINEERING LABORATORY PORT HUENEME CALIFORNIA 93043-5003

Approved for public release; distribution is unlimited.

METRIC CONVERSION FACTORS

Approximate Conversions to Metric Measures

Symbol	When You Know	Multiply by	To Find	Symbol
		LENGTH		
in	inches	*2.5	centimeters	cm
ft	feet	30	centimeters	cm
yd	yards	0.9	meters	m
mi	miles	1.6	kilometers	km
		AREA		
in^2	square inches	6.5	square centimeters	cm^2
ft^2	square feet	0.09	square meters	m^2
yd^2	square yards	0.8	square meters	m^2
mi^2	square miles	2.6	square kilometers	km^2
	acres	0.4	hectares	ha
		MASS (weight)		
oz	ounces	28	grams	g
lb	pounds	0.45	kilograms	kg
	short tons (2,000 lb)	0.9	tonnes	t
		VOLUME		
tsp	teaspoons	5	milliliters	ml
Tbsp	tablespoons	15	milliliters	ml
fl oz	fluid ounces	30	milliliters	ml
c	cups	0.24	liters	l
pt	pints	0.47	liters	l
qt	quarts	0.95	liters	l
gal	gallons	3.8	liters	l
ft^3	cubic feet	0.03	cubic meters	m^3
yd^3	cubic yards	0.76	cubic meters	m^3
		TEMPERATURE (exact)		
°F	Fahrenheit temperature	5/9 (after subtracting 32)	Celsius temperature	°C

*1 in = 2.54 (exactly). For other exact conversions and more detailed tables, see NBS Misc. Publ. 286, Units of Weights and Measures, Price $2.25, SD Catalog No. C13.10:286.

Approximate Conversions from Metric Measures

Symbol	When You Know	Multiply by	To Find	Symbol
		LENGTH		
mm	millimeters	0.04	inches	in
cm	centimeters	0.4	inches	in
m	meters	3.3	feet	ft
m	meters	1.1	yards	yd
km	kilometers	0.6	miles	mi
		AREA		
cm^2	square centimeters	0.16	square inches	in^2
m^2	square meters	1.2	square yards	yd^2
km^2	square kilometers	0.4	square miles	mi^2
ha	hectares (10,000 m^2)	2.5	acres	
		MASS (weight)		
g	grams	0.035	ounces	oz
kg	kilograms	2.2	pounds	lb
t	tonnes (1,000 kg)	1.1	short tons	
		VOLUME		
ml	milliliters	0.03	fluid ounces	fl oz
l	liters	2.1	pints	pt
l	liters	1.06	quarts	qt
l	liters	0.26	gallons	gal
m^3	cubic meters	35	cubic feet	ft^3
m^3	cubic meters	1.3	cubic yards	yd^3
		TEMPERATURE (exact)		
°C	Celsius temperature	9/5 (then add 32)	Fahrenheit temperature	°F

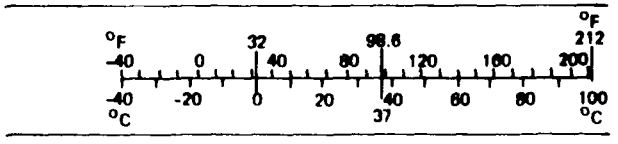

REPORT DOCUMENTATION PAGE

Form Approved
OMB No. 0704-018

Public reporting burden for this collection of information is estimated to average 1 hour per response, including the time for reviewing instructions, searching existing data sources, gathering and maintaining the data needed, and completing and reviewing the collection of information. Send comments regarding this burden estimate or any other aspect of this collection information, including suggestions for reducing this burden, to Washington Headquarters Services, Directorate for Information and Reports, 1215 Jefferson Davis Highway, Suite 1204, Arlington, VA 22202-4302, and to the Office of Management and Budget, Paperwork Reduction Project (0704-0188), Washington, DC 20503.

1. AGENCY USE ONLY *(Leave blank)*	2. REPORT DATE	3. REPORT TYPE AND DATES COVERED
	August 1992	Interim; October 1990 thru September 1991

4. TITLE AND SUBTITLE

THE MECHANISM OF LIQUEFACTION IN LAYERED SOILS

5. FUNDING NUMBERS

C - N47408-89-C-1058

6. AUTHOR(S)

Gregg L. Fiegel, Graduate Research Assistant
Bruce L. Kutter, Associate Professor

7. PERFORMING ORGANIZATION NAME(S) AND ADDRESSE(S)

University of California, Davis
Davis, CA 95616

8. PERFORMING ORGANIZATION REPORT NUMBER

CR 92.009

9. SPONSORING/MONITORING AGENCY NAME(S) AND ADDRESSE(S)

Office of the Chief of Naval Research/ Naval Civil Engineering Laboratory
800 North Quincy Street Code L51
Arlington, VA 22217-5000 Port Hueneme, CA 93043

10. SPONSORING/MONITORING AGENCY REPORT NUMBER

11. SUPPLEMENTARY NOTES

12a. DISTRIBUTION/AVAILABILITY STATEMENT

Approved for public release; distribution is unlimited.

12b. DISTRIBUTION CODE

13. ABSTRACT *(Maximum 200 words)*

Results from six centrifuge model tests are presented. Four of the model tests involve layered soil deposits subject to base shaking; two model tests involve uniform soil deposits of sand subject to base shaking. The layered soil models consisted of a saturated liquefiable fine sand overlain by a layer of relatively impermeable silica flour (silt). Pore water pressures, accelerations, and settlements were measured during all six tests. Results from the model tests involving layered soils suggest that during liquefaction, a water interlayer or very loose zone of soil develops between the sand and the silt due to the difference in permeabilities. Soil volcanos or boils were seen on the surface for all four of these layered model tests. The locations of these boils, in each test, were found concentrated in the weakest zones of the overlying silt layer; cracking of the weak silt zones provided a release or a vent for the excess pore water pressure generated as a result of particle rearrangement in the liquefiable fine sand.

14. SUBJECT TERMS

Dynamic testing, geotechnical centrifuge models, liquefaction, pore pressure, sand boils, failure mechanisms

15. NUMBER OF PAGES

34

16. PRICE CODE

17. SECURITY CLASSIFICATION OF REPORT	18. SECURITY CLASSIFICATION OF THIS PAGE	19. SECURITY CLASSIFICATION OF ABSTRACT	20. LIMITATION OF ABSTRACT
Unclassified	Unclassified	Unclassified	UL

THE MECHANISM OF LIQUEFACTION IN LAYERED SOILS

Gregg L. Fiegel [1] and Bruce L. Kutter [2]

[1,2] - Graduate Research Assistant and Associate Professor, respectively;
University of California, Davis

ABSTRACT: Results from six centrifuge model tests are presented. Four of the model tests involve layered soil deposits subject to base shaking; two model tests involve uniform soil deposits of sand subject to base shaking. The layered soil models consisted of a saturated liquefiable fine sand overlain by a layer of relatively impermeable silica flour (silt). Pore water pressures, accelerations, and settlements were measured during all six tests. Results from the model tests involving layered soils suggest that during liquefaction a water interlayer or very loose zone of soil develops between the sand and the silt due to the difference in permeabilities. Soil volcanos or boils were observed on the surface for all four of these layered model tests. The locations of these boils, in each test, were found to be concentrated in the weakest zones of the overlying silt layer; cracking of the weak silt zones provided a release or a vent for the excess pore water pressure generated as a result of particle rearrangement in the liquefiable fine sand.

INTRODUCTION

Recent earthquakes in Northern California and the Philippines have helped to emphasize the importance of geotechnical earthquake engineering. Ground failures and, in particular, liquefaction were responsible for the loss of many lives and millions of dollars worth of damage in both of the above mentioned earthquakes (EERI 1990; Wieczorek et. al. 1991). Studying the phenomenon of liquefaction is, however, difficult due to the fact that earthquakes occur relatively infrequently and are difficult to predict with any accuracy.

As an alternative, dynamic centrifuge modeling can be used to study the effects of earthquakes on soil. The centrifuge permits small scale models to be tested in a controlled environment. Realistic scaled earthquake time histories can be applied to centrifuge models, and small scale instrumentation can be used to study the dynamic response.

In particular, the centrifuge can be used to study failure mechanisms. The ability to study failure mechanisms makes the centrifuge a valuable tool for the geotechnical engineer; a fundamental understanding of the underlying mechanism of any geotechnical engineering problem is essential before more thorough investigations can proceed and analytical models can be developed. This paper examines the mechanism of soil liquefaction in layered soil deposits along with the mechanism of sand boil generation. Work for the paper was done as part of the VELACS project (Arulanandan et. al. 1991).

LIQUEFACTION MECHANISMS

During an earthquake event, cyclic shear strains in the deposit cause a progressive build-up of pore water pressure. In the case where this pore water pressure reaches a value equal to the initial confining pressure, liquefaction is said to have occurred. Detailed summaries with regard to this phenomenon are presented by Seed (1979), Ishihara (1985), and the National Research Council (1985).

In the condition of zero effective stress, or liquefaction, the soil particles or grains do not support one another and therefore act as a suspension. Eventually, the soil particles of this suspension tend to settle due to the fact that they are heavier than water; the rate of this settlement or sedimentation is restricted by the fact that water must flow upward around the soil particles. In a condition of zero effective stress, the principle of effective stress indicates that the upward hydraulic gradient due to the generated excess pore water pressure will be equal to the critical hydraulic gradient, i_{crit} , where i_{crit} equals γ_b/γ_w. Assuming that Darcy's law of flow is valid, one can conclude that the upward flow of water will move with an apparent velocity of $v \approx k\, i_{crit}$ where k is the permeablility of the soil. If there is no downward drainage through the deposit, then this relative velocity of water flow at the surface, by continuity, must be equal to the velocity of settlement of the soil surface (Florin and Ivanov 1961; Heidari and James 1982; Whitman et. al. 1982; and Scott 1986). Schofield (1981) examined this flow concept in more detail; he has suggested that while in a condition of very small effective stresses, microcracks or fissures may form within the soil which may cause a dramatic increase in the apparent permeability of the soil.

It is rarely the case, however, to find naturally occurring uniform deposits of liquefiable soil that extend from the surface to some significant depth; stratification normally exists within field soil deposits. Often, liquefiable soil deposits are overlain by dense sands, topsoils, and other less permeable soils. This stratification can have a dramatic effect on the liquefaction mechanism outlined previously. Overlying deposits of less permeable soils can restrict the escape of excess pore water pressure generated in the liquefiable soil during the earthquake.

During liquefaction of a layered soil deposit, the velocity of water flow through the overlying less permeable soil is much slower relative to the velocity of flow through the liquefied sand. Numerous authors have pointed out that this difference in velocity could result in an accumulation of water in the form of a water gap or very loose zone of soil at the interface (Whitman 1985; National Research Council 1985; and Seed 1987). In shaking table tests involving stratified sand layers, Liu and Qiao (1984) have observed a water interlayer below a relatively impervious zone of soil.

Kutter and Fiegel (1991), taking into account this concept of a water interlayer between different permeability soils, have described a mechanism applicable to liquefaction in layered or stratified soil deposits. Two separate mechanisms, as observed in centrifuge tests, are shown in Figure 1. After the generation of a water gap or interfacial loose zone of soil in the stratified deposit, the overlying less permeable soil could, as shown in the figure, temporarily float. In this condition, pore water pressure in the water gap or loose soil zone is, by equilibrium, equal to the total overburden pressure. Thus, the overlying soil, regardless of its type, is subject to the critical hydraulic gradient. The critical hydraulic gradient leads to a condition of zero effective stress; therefore, the overlying soil deposit is severely weakened and likely to break apart.

The failure of the upper layer of less permeable soil is likely to occur at thin zones in the deposit (Ishihara 1985). This mechanism is depicted in both (a) and (b) of Figure 1. In (a), a small mound of silt overlies a level sand deposit; as a result, a thin, less heavy layer of silt exists at the left and right sides of the model. In (b), the silt is very nearly level, but the sand is sloped towards the center. This geometry creates a thin or light layer of silt at the center of the model. As shown in both figures, heavier, thicker zones of the upper

DTIC QUALITY INSPECTED 1

Dist | Avail and/or Special
A-1

soil layer will eventually fall through the water gap or loose zone and force water towards the lighter or thinner portions of the deposit. In these thin areas the upper soil layer will bulge due to the local influx of interfacial water, and flow velocities will increase due to the weaker resistance along the flow path. The bulging, in combination with increased flow velocities, greatly reduces the strength of the overlying deposit. As a result, the overlying deposit cracks or fails.

The cracks in the overlying deposit provide a vent for the pore water accumulating at the interfacial zone. Eventually, if flow velocities through these cracks are high enough, particles of soil will be eroded by the flow. An enlargening orifice will result along with a concomitant increase in flow velocities, and a soil volcano or sand boil will occur at the surface of the deposit (Kutter and Fiegel 1991).

The problem can be further complicated if the stratified deposit is not perfectly level. The presence of water at the interface between the two soil layers results in a dramatic reduction in the sliding resistance of the liquefied layer. As a result, lateral spreading or debris flows may result. Youd (1984) and the National Research Council (1985) have described such a mechanism where the overlying less permeable soil cracks, breaks up, and flows laterally even for cases where the slope is very gentle. Arulanandan et. al. (1988) have observed a flow type failure in a centrifuge experiment involving a layered embankment.

CENTRIFUGE TESTS

Listed in Table 1 are the six centrifuge tests that were performed for this study; the six tests are referred to as GF3, GF4, GF5, GF6, SL1, and SL2. All six tests were performed on the Schaevitz centrifuge at U.C. Davis at a centrifugal acceleration of 50g.

The Schaevitz centrifuge is equipped with a servo-hydraulic actuator (shaker) that is capable of reproducing realistic scaled earthquake time histories and spectra (Chang 1990). Two different time histories or base motions were used to shake the models tested in this study. The first time history was an approximate sine wave with 10 uniform cycles of predominantly 1 Hz base acceleration; the second time history was a simulated El Centro earthquake with the motion scaled to produce a peak base acceleration of about 0.6g. Table

1 reveals the type of base motion used for each centrifuge test.

Three different soils were used in the model tests examined in this paper: a coarse sand with a mean grain size of 0.4 mm (base sand), a fine sand with a mean grain size of 0.13 mm (Nevada sand), and a silica flour (silt). A test by test breakdown of the soil data is included in Table 1 while a description of each soil is included in Table 2.

Pore water pressure transducers, accelerometers, and linear variable differential transformers (LVDT's) were used to measure soil response in each of the model tests. Each test was performed using the same container or model box. This box was 22" long, 11" wide, and 7" high and had an aluminum base, aluminum end walls, and clear plexiglass side walls. The clear plexiglass walls permitted a side view of the model during each centrifuge test.

MODEL CONSTRUCTION

Each of the six tests, in prototype terms, simulate level soil deposits. To simulate a level deposit in a small centrifuge, a curved model must be constructed; this curved model is needed so as to compensate for the radial acceleration field generated by the centrifuge. For each of the tests presented, the base sand, Nevada sand, and silica flour (silt) layers have all been curved to radii corresponding to the radius of the centrifuge.

The first part of building the model involved the base sand layer. This layer, made of coarse sand, was used to provide a dense, curved base for the model. A plexiglass curving tool was used to accurately form the coarse sand layer to the proper radius of curvature. The base sand was placed in a dense state at nearly 100% relative density; this fact was confirmed for each test: no recognizable settlement of the base sand layer was observed after shaking.

After the base sand was placed, the Nevada sand layer was added to the model. The Nevada sand was dry pluviated through a screen with a plastic funnel to create a layer with a void ratio of 0.67; this void ratio led to dry density of 100.1 pcf and a relative density of 60%. Like the base sand layer, the Nevada sand was smoothed to the proper curve after the desired height had been reached. It should be noted that the pluviation process was periodically stopped so that instrumentation could be placed in the model. This

instrumentation included pore water pressure transducers, accelerometers, and footings for the LVDT cores. The footings used to support the LVDT cores were fabricated out of plexiglass and balsa wood. An effort was made to make these LVDT supports neutrally buoyant with respect to the surrounding model soil. This was done to insure that the supports would not sink into the model soil during shaking. Previous settlements recorded in centrifuge liquefaction experiments have not been emphasized since it was not clear that the LVDT supports did not sink into liquefied soil (Whitman et. al. 1982).

Following the creation of the base sand and Nevada sand layers, the model was saturated with water. First, the top of the model box was covered with an aluminum plate. A vacuum of 28" to 30" of Mercury was then applied to the sealed model box. Once a full vacuum was reached, the model box was flooded with CO_2 gas and allowed to sit for five minutes. After five minutes, the CO_2 was removed by a vacuum and the entire CO_2 saturation process was repeated. Next, a vacuum was applied once more and de-aired water was allowed to drip in through the top of one end of the model box.

After saturation was completed, silica flour (silt) was added to the model; most of this silica flour was added at 1g. The silica flour was mixed with de-aired water to form a slurry with a water content of 50%. The slurry was then poured slowly into the model. Pouring the slurry into the model in this fashion caused a visible layering effect to occur in the silt deposit which was helpful when examining post-earthquake deformations. Of course, pouring the silt slurry into the model in a 1g environment created a flat surface that did not simulate level ground on the centrifuge. To produce the curved shape needed for the silt layer, a final mixture of silt slurry was poured into the model, and the centrifuge was quickly brought up to speed. The acceleration field generated by the centrifuge caused the silt particles to settle out in the curved shape desired.

CENTRIFUGE SCALING LAWS

The scaling laws for dynamic centrifuge modeling are described in some detail by Schofield (1981). Scaling laws important in this study are summarized in Table 3. A well known conflict exists between the time scale factors used for dynamic shaking and pore

pressure dissipation. Since water was used as the pore fluid in all model tests, the models do not correspond to prototypes made of the same soil; the model soils actually simulate soils with a permeability N times greater (Tan and Scott 1985). Scaling permeability, k, in this manner allows for 1/N scaling of time, t. Also, this scaling implies that, from the standpoint of permeability, the fine sand and silt in the model more closely represent a coarse sand and silty sand in prototype. After multiplying by 50, the prototype permeabilities of the Nevada sand and silica flour (silt) are 1.5×10^{-1} cm/sec and 1.5×10^{-4} cm/sec, respectively.

MODEL CONFIGURATIONS

Model configurations for the six different centrifuge tests are shown in Figures 2 and 3. Test GF3 simulated a level, layered soil deposit with silt overlying liquefiable sand. The silt layer was 2" thick, and the sand layer was 1.75" thick. LVDT's were placed on the silt surface in two locations and at the silt-sand interface in two locations.

Test GF4 simulated a level soil deposit with silt overlying liquefiable sand; however, the model configuration was considerably different from GF3. For test GF4, an island or mound of Nevada sand was constructed. The sand layer was again level in the central region of the model; however, thicknesses were greatly reduced along the four sides of the box (see test GF4, Figure 2). In the center of the GF4 model, the silt layer was 1" thick and the sand layer was 1.75" thick. A total of five LVDT's were placed on the surface of the silt along the width near the centerline (into the page of the figure).

The models used in tests GF5 and GF6 were constructed in much the same manner as for test GF4. Again, the silt layer was level and a mound of sand was used. However, as shown in Figures 2 and 3, the sand surface was not level. The sand layer sloped up toward the center of the model at an angle of approximately 6 degrees and created a 4" wide level section of sand. The resulting model had a layer of silt that was thinnest at the center: 1.0" in GF5 and 1.25" in GF6. Six LVDT footings were placed on the silt surface in the length-wise direction along the centerline; Figures 2 and 3 show this configuration.

Prior to shaking the models used in tests GF4, 5, and 6, the water table was lowered

to the surface of the deposit and a thin layer of black silt was placed on the white silt to mark the initial ground surface. The photograph in Figure 3 shows this thin black silt layer after it has been dusted onto the surface. The dashed line on the plexiglass window represents the approximate location of the sand mound inside the silt.

The SL models simulated uniform, non-layered sand deposits; they are not shown in Figures 2 or 3. In both model tests, the sand layer was 4" thick. In test SL1, the model was dry and included LVDT's along the surface. In test SL2, the model was saturated and included a full set of instrumentation. Instruments used in the SL model tests were placed in locations comparable with tests GF5 and GF6.

TEST RESULTS

Centrifuge tests were run following the construction of the each of the models. Prior to shaking each model, they were allowed to consolidate at 50g for approximately 20 minutes. Acceleration, pore water pressure, and settlement data for the six tests are presented in the following sections; a detailed summary of the data is found in Fiegel (1992).

Considerable edge effects developed in test GF3. In test GF3 both the Nevada sand and silt layers were constructed against the side walls of the model box. The walls, unfortunately, provided a flow path for water in the model; as a result, a considerable amount of boiling occurred along the plexiglass walls during the shaking event. A video camera mounted on the swing bucket of the centrifuge recorded this boiling.

In test GF4 a mound of sand was constructed so that boiling could be directed away from the side walls of the model box. However, as shown in Figure 2, the surface of the deposit for test GF4 was not completely level in prototype terms. This non-level surface led to the silt layer being thinnest near the right and left ends of the model, and as a result, boiling occurred in these areas. As reported in Kutter and Fiegel (1991), a relatively large boil occurred at point A in Figure 2. Unfortunately, however, boiling did not occur in the center of the model where most of the instrumentation was focussed. This problem of a non-level prototype surface arose in test GF4 because of the difficulty involved in attempting

to generate the curved model surface. Several attempts at generating this properly curved surface are usually required when constructing the model.

In tests GF5 and GF6 the layered soil model was further modified: the Nevada sand layer was sloped to produce a thin silt layer in the middle of the box. This sloping mound of sand was created in an attempt to force boils to occur in a relatively small area at the center of the model. As shown later, the attempt was successful. The actual, scaled silt surface profiles prior to shaking for tests GF5 and GF6 are shown in the model configuration sketches (Figures 2 and 3). The silt surfaces in these two cases, unlike in test GF4, very nearly simulate a level prototype.

It has been pointed out that edge or boundary effects caused some problems during the course of this study and that an effort was made to correct them. Whitman and Lambe (1986) have examined the boundary effects that rigid side walls create when modeling the liquefaction phenomenon. They state that end walls have a significant effect on soil stresses a distance of 1.5 to 2 times the soil depth from the side wall. The average depth for models used in this study is about 3.5"; therefore, edge effects should be significant about 7" from each side wall. For each of the six centrifuge tests, accelerometers and pore pressure transducers were placed clear of these 7" areas.

MODEL ACCELERATIONS

Accelerations were measured at several locations for each of the models examined in this study. The acceleration time histories for tests GF4, GF6, and SL2 are shown in Figure 4. The plots are presented in prototype terms.

The bottom acceleration record for each of the tests shows the base horizontal motion recorded. The base motion for test GF4 simulated a sine wave while the base motion for tests GF6 and SL2 simulated an El Centro earthquake. In test GF4 the duration of the base motion was approximately 10 seconds and the peak horizontal acceleration at the base was 0.42g. In tests GF6 and SL2 the duration of the base motion was approximately 31 seconds and the base peak horizontal accelerations were 0.62g and 0.64g, respectively. The accelerometer in the base sand for test SL2 malfunctioned; therefore,

there is no record. Also, the ground accelerations measured in the uniform sand layer (SL2) were measured at locations comparable with tests GF4 and GF6.

In tests GF4 and GF5, accelerations in the silt follow the input motion fairly well for the first few cycles; however, as shaking proceeds, the silt accelerations damp out severely and are negligible for the remainder of the event. Comparison with SL2 data shows that an accelerometer in a comparable position generates a significant acceleration record for the entire event. In tests GF4 and GF6, the silt layer is effectively isolated from the base, hence the low accelerations. This fact provides evidence in favor of the existence of a water interlayer between the sand and silt during liquefaction. In tests GF4 and GF6, the silt layer, after a few cycles of shaking, is resting or "floating" on a layer of water. Water cannot withstand a shear stress; thus, shear waves generated from the base motion are effectively damped out in the silt layer.

Another important point regarding the accelerations are the large spikes observed in the sand layer for all three tests. These spikes are especially apparent for the sand acceleration record of test GF4. The maximum input acceleration at the base was 0.42g, yet accelerations of about 1.75g were recorded in the Nevada sand layer. The sand acceleration record for test GF4 lags approximately 0.1 seconds behind the input base motion; also, this same record shows an underlying acceleration record with an amplitude of about 0.15g indicating that the deposit has most likely liquefied. The large spikes in the record fall between the smaller peaks of the liquefied record. These spikes may be explained by examining the q-p stress path observed for cyclic triaxial tests on sand. As the pore water pressures increase due to the shaking, the sand moves towards liquefaction. Eventually the stress path for the sand crosses the phase transformation line (PTL), and as a result, the sand dilates. This dilation could cause a locking of the soil grains. This locking of the grains due to dilation combined with the acceleration in the opposite direction of motion due to the time lag could cause a large spike in the record.

MODEL PORE WATER PRESSURES

Pore water pressure records for tests GF4, GF5, and SL2 are shown in Figures 5, 6,

and 7. The vertical axis for these plots represents pressure in psi; the horizontal axis is time in seconds. Model time values have been multiplied by N to represent a prototype in dynamic terms. The previously outlined difficulties in accurately scaling the dissipation of pore water pressure should be considered. As stated earlier, from the standpoint of pore pressure dissipation, the sand and silt represent prototype soils with larger permeabilities than the model soils.

A description of the location of each transducer is shown on each pore pressure trace. Measured locations were made before and after each test. The initial measurements have been used to calculate an initial overburden pressure value, σ_{vo}'; this value is shown for each pore pressure trace. The excess pore water pressure developed during shaking can be compared with σ_{vo}' to check if the deposit has liquefied.

It appears that the sand layer reaches a condition of zero effective stress ($u/\sigma_{vo}' \approx 100\%$) and liquefies for each test. In most cases the excess pore water pressure appears to exceed the initial overburden value; this discrepancy arises because of settlement of the transducer. Evidence of transducer settlement is visible on the GF4, GF5, and SL2 plots. The nearly flat record found at the end of each pore pressure trace (Figures 5, 6, and 7) indicates that excess pore pressures generated during the shaking event have very nearly dissipated, yet the excess pore water pressure has not returned to the initial value. This apparent inconsistency is explained by settlement of the transducer relative to the ground water table. The settlement of the transducer relative to the ground water table can be calculated by dividing the residual excess pore water pressure after dissipation, Δu_r, by the unit weight of water. In test SL2, the residual pore pressure for the top pore pressure trace is 0.48 psi; therefore, the calculated settlement, in prototype terms, is 13.3 inches. Displacement transducers used during the same test recorded a little over 14" of surface settlement at the center of the model. The agreement between the two values supports the idea that the residual pore pressure, Δu_r, is a result of transducer settlement. In addition, this settlement helps to explain why some of the measured pore pressures exceed σ_{vo}'; if the final pore pressure was taken as zero instead of the initial pore pressure, the calculated excess pore pressures would be less.

In tests GF4 and GF5 the pore pressure results and transducer settlement

measurements are further complicated by the fact that the water table rises during shaking. As stated, the water table was lowered to the silt surface in tests GF4, GF5, and GF6. In test GF5 the water table was lowered below the silt surface, but the silt remained saturated by capillarity. Shaking the model destroyed this capillary tension and caused a rise in the water table. Evidence for this rise in the water table is shown in the base sand pore water pressure trace for test GF5. The base sand transducer did not settle during the shaking event, yet a residual excess pore water pressure has been measured.

Overall, results from tests GF4 and GF5 show that pore pressure generation in layered soil deposits is quite different from pore pressure generation in uniform soil deposits (SL2). In test SL2 pore pressures rise rapidly during shaking and dissipate rapidly following the event. In tests GF4 and GF5 pore pressures build up rapidly in the sand; however, pore pressure build up in the silt is slower. This build up in the silt is slower because water is collecting at the interface between the silt and sand.

Pressures in the bottom of the sand layer begin to dissipate immediately after the event in test GF4 and during the event in test GF5. The time at which pore water pressure dissipation begins corresponds to the solidification of the soil. A solidification front proceeds upward through the sand deposit and is clearly visible in test GF4; the front reaches the transducer at the top of the sand at t = 18 seconds, approximately 5 seconds after starting at the bottom. Scott (1986) has studied this concept of a solidification front.

In test GF4, the dissipation due to solidification eventually begins to level off at about 23 seconds. A similar stabilization occurs in test GF5. During this flat period of the record, the silt layer is floating on an interface of water or loose zone of soil; the silt, acting as a heavy fluid, is transferring its weight through the interfacial water and into the sand. The pressure due to the floating silt layer can be calculated by knowing both the buoyant unit weight and thickness of the silt. The actual (corrected) pore water pressure at the top of the sand can be found by subtracting Δu_r from the stable u value. Both of these values have been calculated and are shown for the 'Top of Sand' plots in both Figures 5 and 6. The values calculated for both tests show excellent agreement.

Eventually, as shown for both tests GF4 and GF5, the pore pressures begin to dissipate again. At this point the silt layer has ruptured. The silt layer fails or cracks and

pore pressure is vented to the surface of the deposit via soil volcanos or boils allowing dissipation to be accelerated. Boils of this sort were observed on a video tape for tests GF4, GF5, and GF6; the time of occurrence for these boils corresponded with the dissipation observed in the pore pressure records.

MODEL SETTLEMENTS

Settlement and swell time histories measured by LVDT's for all six tests are shown in Figure 8. Both displacement and time values have been scaled (multiplied by 50) so as to represent prototype values.

Plot (a) includes LVDT data recorded for test GF3. The model configuration for test GF3 included four LVDT's: two at the silt-sand interface and two on the surface. The two interface records along with the surface-center record are shown. All the LVDT's recorded only settlement. A considerable amount of settlement occurred in the Nevada sand layer; approximately 24 seconds into the record, the interface-sand LVDT has recorded a total of 6" of settlement.

Strictly settlement was also recorded for test GF4 (Figure 8b). In this test, five LVDT's were located along centerline of the surface of the silt in the width-wise direction; the plot shows data recorded by the front, front-inner, and center LVDT's. Similar plots exist for the back and back-inner LVDT's. Recall that for this test boiling occurred at the left and right sides of the model and not near the LVDT's placed along the width at the centerline.

As shown in plots (c) and (d), settlement and swell were recorded for both tests GF5 and GF6. In these tests, LVDT's were placed on the silt surface along the length of the box; also, the sand layer was sloped upwards toward the center of the model so that the silt layer was thinnest at this point (see Figures 2 and 3). Both test GF5 and GF6 show that the left center LVDT recorded significant swell. In test GF5 this swell was about 5" while in test GF6 this swell was about 11". At t=55 seconds this swell has peaked for test GF5; however, for test GF6, the swell continues for about 40 more seconds. Note that for both tests, high amplitude, oscillatory motion was recorded for the left LVDT. It is clear that the

left end wall of the model box has some effect on measured settlements; however, the end wall does not seem to have this same effect on settlements measured near the center of the model.

The final plots of Figure 8 show the LVDT records for tests SL1 and SL2. As shown in plot (e), no significant settlement, swell, or oscillation was recorded for the dry uniform sand layer tested in SL1. However, data recorded for test SL2 reveals that significant settlement of the sand layer occurs when it is saturated. The left-center LVDT for test SL2 recorded a settlement of over 14" while the left LVDT recorded a settlement of about 7".

For the settlement plots presented, the rate of settlement as expected by Darcy's law does not occur. The settlement rates for tests GF3, GF4, and SL2 are all approximately 1.5 cm/sec. However, the expected settlement rate, k, is 1.5×10^{-1} cm/sec for the Nevada sand and 1.5×10^{-4} cm/sec for the silt (after scaling). The differences are large; therefore, water must be draining out of pipes or fissures in the soil mass. The data further suggests that the permeability of the soil may increase dramatically as the hydraulic gradient approaches its critical value.

MODEL SURFACE PROFILES

Settlement and swell data has been used to create surface profile plots for tests GF5, GF6, and SL2; these plots are shown in Figure 9. The three plots show surface settlement or swell in prototype inches along the vertical axis; the model box length is shown in prototype scale along the horizontal axis. The individual profiles shown in each plot represent silt surface profiles measured by the LVDT's at a particular time during or after the shaking event. The time, t, for each particular profile is shown and represents prototype time after shaking begins. For example, in test GF5 the line with a 15 under it represents the silt surface profile 15 seconds after the shaking event begins.

The surface profiles generated for test GF5 show that a bulge forms in the center are[illegible] the model near the end of the shaking event. Settlement at the surface is first recorded at 15 seconds, shortly after the event begins. The center of the model, however, begins to bulge after this time and eventually reaches a peak at 44 seconds; shaking stops

at about t=32 seconds. As evident by the recording shown for the right-center LVDT, bulging of this magnitude was not entirely anticipated. In fact, at t=44 seconds, the right center LVDT went completely off scale and no data was recorded; consequently, the data point at t=44 seconds for this LVDT has been estimated and is denoted by two question marks.

The bulging in test GF5 is consistent with the liquefaction mechanism described in Figure 1(b). During the shaking event, the Nevada sand layer liquefies and subsequently settles. As the sand settles, water flows towards the surface; however, the water is trapped by the less permeable silt layer. Heavier, thicker zones of the silt at the left and right sides of the model may settle rapidly and force water at the interfacial boundary to flow toward the center where the silt is thin; consequently, a bulging occurs. In the case of test GF5, flow toward the thinnest part of the silt caused bulging and eventual ground failure or boiling. This failure, in turn, led to a rapid release of pore pressure and large local settlements. Large local settlements are evident on the GF5 surface profile plot. Settlement of the deposit eventually stops at t=335 seconds; at this time, the maximum settlement of the deposit is about 14".

The scenario described above for test GF5 is also evident in the surface profile record of test GF6; note that nearly the same amount of settlement was recorded at the center of the model. Some slight differences exist, however, when comparing other data from tests GF5 and GF6. In particular, for test GF6, the time from the beginning of the shaking event until the time at which boiling occurred was approximately 51 seconds longer than that of test GF5. As shown, boiling, or failure of the silt layer, does not occur until t=95 seconds or approximately 63 seconds after the shaking event is over. The 25% thicker silt layer in GF6 is most likely responsible for the extra time required for boiling.

The final profile shown in Figure 9 is the profile associated with test SL2, the uniform sand layer; this profile enables comparison with the layered soil deposit profiles shown for tests GF5 and GF6. In test SL2 there was no dramatic swelling or bulging associated with the sand layer; only settlements were recorded. The maximum settlement recorded was about 15". An edge effect is also clear in test SL2; the settlement at the ends is much less than that in the center of the model.

In each of the surface profiles presented, some swelling occurs at the right side of the model. If each of the models represent level prototypes, then this swelling should not occur. It has been found, however, that the silt surface is not actually level before shaking. Before spin-up, the model surfaces for tests GF5, GF6, and SL2, as measured, simulated level prototypes (within 0.05 inches); however, starting the centrifuge in motion caused a small amount of movement of the soil in the left-hand direction. With this movement, the left side of the model became slightly higher than the right side. As a result, the model soil tended to flow to the right during shaking and caused a small amount of swell. Observed right to left movement of the soil during spin-up is greater in tests GF5 and GF6 than in test SL2; therefore, the amount of swell recorded by the right LVDT is larger.

SOIL VOLCANOS OR BOILS

After shaking, each model was dissected and cross-sections were photographed. Photographs showing the cross-sections of soil volcanos or boils that occurred in tests GF5 and GF6 are shown in Figure 10. In both tests the boiling occurred in the center of the model where the silt layer was thinnest.

The photos for tests GF5 and GF6 show that soil particles were carried to the model surface and deposited over top of the black silt layer. In test GF5, the boil, as shown, carried both silt and sand to the surface of the model; however, for test GF6, only silt was carried to the surface. The difference in thickness of the silt layer for tests GF5 and GF6 could explain variation.

Subsurface erosion of the silt and sand layers is evident for both tests GF5 and GF6. The photographed cross-sections (Figure 10) show that the once horizontal layering in the silt is now curved downward in the vicinity of the boil. Both sand and silt particles in test GF5 and only silt particles in test GF6 were carried or eroded from the interface area surrounding the boil. Large local settlement was consequently found at the surface of the deposit. Through the dissection process, it was found that this local settlement was bowl shaped. It should be noted that the boils in tests GF5 and GF6 were observed and recorded by video cameras mounted inside the centrifuge. In some cases, soil was observed to spurt

above the silt ground surface in the form of a mini-geyser.

SUMMARY AND CONCLUSIONS

The results of the six centrifuge tests presented are consistent with the liquefaction mechanisms outlined at the beginning of this paper. Liquefaction of a uniform soil deposit is a complex phenomenon; however, the phenomenon is further complicated for layered soil deposits. It has been found that:

1. An overlying, relatively impermeable soil tends to restrict the escape of pore water produced by the settlement of an underlying liquefiable sand layer. This can result in the formation of a water gap or a very loose zone of soil at the interfacial boundary. Pore water pressure, LVDT, and acceleration records from the centrifuge tests presented in this paper provide evidence in favor of the existence of this water gap or loose zone of soil.

2. The presence of a water gap or loose soil zone leads to abnormal shifting or movement of the overlying soil layer. Thicker zones of the overlying soil fall through the water gap and force water to thinner, weaker zones. This action may result in a temporary bulging of the ground surface at some locations; rapid settlements may occur at other locations.

3. The bulging action of the overlying soil and high pressure gradients tend to weaken the overlying soil layer. Inevitably, cracks or fissures will form in the overlying layer thereby allowing the rapid escape of interfacial water. The relatively high velocity of water through these cracks causes erosion and piping which leads to boils on the surface of the deposit.

4. The development of cracks in the overlying soil results in a higher apparent permeability of the soil. This increase in permeability significantly effects the amount of time that a soil deposit can be in a liquefied state. Also, settlement velocities based on soil permeability are higher than expected, indicating that k may change during the shaking event.

Overall, the geotechnical centrifuge can be a valuable tool when studying the mechanisms involved in soil liquefaction of both uniform and layered soil deposits; field aspects of the liquefaction phenomenon, in particular sand boils, were observed in a model environment. Nearly identical centrifuge model configurations were found to produce very similar results indicating that centrifuge modelling can be both repeatable and reliable.

ACKNOWLEDGMENTS

The work performed in this study was supported by the National Science Foundation (Grant No. BCS89-12074) and the Naval Civil Engineering Laboratory. The support of these organizations is gratefully acknowledged. The writers would also like to thank Dan Wilson for performing the SL centrifuge tests, Bill Sluis and Dr. X.S. Li for their technical support, and Professors I.M. Idriss and J.S. DeNatale for their critical review of this manuscript.

APPENDIX I. REFERENCES

Arulanandan, K., Yogachandran, C., Muraleetharan, K.K., Kutter, B.L., and Chang, G.S. (1988) "**Seismically Induced Flow Slide on a Centrifuge,**" Journal of Geotechnical Engineering, ASCE, Vol 114, No. 12, pp. 1442-1449.

Arulanandan, K., et. al. (1992) "**Project VELACS - Verification of Liquefaction Analysis by Centrifuge Studies,**" In preparation for publication, Journal of Geotechnical Engineering, ASCE.

Chang, G.S. (1990) "**Centrifugal and Numerical Modeling of Soil-Pile-Building Interaction During Earthquakes,**" PhD Thesis, University of California, Davis.

EERI (1990) "**Loma Prieta Earthquake Reconnaissance Report,**" Earthquake Spectra, Supplement to Vol. 6.

Fiegel, G.L. (1992) **Untitled**, Master's Thesis in preparation, University of California, Davis.

Florin, V.A. and Ivanov, P.L. (1961) "**Liquefaction of Saturated Sandy Soil,**" Proceedings of the 5th International Conference of Soil Mechanics and Foundation Engineering, Paris, p.106.

Heidari, M. and James, R.G. (1982) "**Centrifuge Modelling of Earthquake Induced Liquefaction in Saturated Sand,**" Proceedings from the Conference on Soil Dynamics and Earthquake Engineering, Vol. 1, A.A. Balkema Publishers, Rotterdam, Netherlands, pp. 271-281.

Ishihara, K. (1985) "**Stability of Natural Deposits During Earthquakes,**" Proceedings of the Eleventh International Conference on Soil Mechanics and Foundation Engineering, A.A. Balkema Publishers, Rotterdam, Netherlands, pp. 321-376.

Kutter, B.L. and Fiegel, G.L. (1991) "**Mechanism of Sand Boil Formation in Layered Soils as Observed in Centrifuge Tests,**" Proceedings from the Third Japan-U.S. Workshop on Earthquake Resistant Design of Lifeline Facilities and Countermeasures for Soil Liquefaction, Technical Report NCEER-91-0001, pp. 279-292.

Liu, H. and Qiao, T. (1984) "**Liquefaction Potential of Saturated Sand Deposits Underlying Foundation of Structure,**" Proceedings of the Eighth World Conference on Earthquake Engineering, Vol III, San Francisco, pp. 199-206.

National Research Council (1985) "**Liquefaction of Soils During Earthquakes,**" Report No. CETS-EE-001, Committee on Earthquake Engineering, National Academy Press, Washington D.C.

APPENDIX I. REFERENCES (CONT.)

Scott, R.F. (1986) "**Solidification and Consolidation of a Liquefied Sand Column,**" Soils and Foundations, JSSMFE, Vol. 26, No. 4, pp. 23-31.

Seed, H.B. (1979) "**Soil Liquefaction and Cyclic Mobility Evaluation for Level Ground During Earthquakes,**" Journal of the Geotechnical Engineering Division, ASCE, Vol. 105, No. GT2, pp. 201-255.

Seed, H.B. (1987) "**Design Problems in Soil Liquefaction,**" Journal of Geotechnical Engineering, ASCE, Vol. 113, No. 8, pp. 827-845.

Schofield, A.N. (1981) "**Dynamic and Earthquake Geotechnical Centrifuge Modeling,**" Proceedings from the International Conference on Recent Advances in Geotechnical Earthquake Engineering and Soil Dynamics, University of Missouri, Rolla, Missouri, Vol. 3, pp. 1081-1100.

Tan, T.S. and Scott, R.F. (1985) "**Centrifuge Scaling Considerations for Fluid-Particulate Systems**, Geotechnique, Vol 35, No. 4, pp. 461-470.

Whitman, R.V. (1985) "**On Liquefaction,**" Proceedings of the 11th International Conference on Soil Mechanics and Foundation Engineering, Vol. 4, San Francisco, pp. 1923-1926.

Whitman, R.V. and Lambe, P.C. (1986) "**Effect of Boundary Conditions Upon Centrifuge Experiments Using Ground Motion Simulation,**" Geotechnical Testing Journal, GTJODJ, Vol. 9, No.2, pp. 61-71.

Whitman, R.V., Lambe, P.C., and Akiyama, J. (1982) "**Consolidation During Dynamic Tests on a Centrifuge,**" Preprint 82-063, ASCE National Convention, Las Vegas, Nevada.

Wieczorek, G.F., Arboleda, R., and Tubianosa, B. (1991) "**Liquefaction and Landsliding from the July 16, 1990, Luzon, Philippines Earthquake,**" Proceedings from the Third Japan-U.S. Workshop on Earthquake Resistant Design of Lifeline Facilities and Countermeasures for Soil Liquefaction, Technical Report NCEER-91-0001, pp. 39-55.

Youd, T.L. (1984) "**Geologic Effects - Liquefaction and Associated Ground Failure,**" Proceedings from the Geologic and Hydrologic Hazards Training Program, Open File Report 84-760, U.S. Geological Survey, Menlo Park, California.

APPENDIX II. NOTATION

The following symbols are used in this paper:

i_{cnt} = critical hydraulic gradient

γ_b = effective unit weight

γ_w = unit weight of water

v = velocity of water flow (Darcy)

k = permeability

e = void ratio

D_{50} = mean grain size

D_r = relative density

N = scaling factor

$( )_m$ = model variable

$( )_p$ = prototype variable

a = acceleration

σ_{vo}' = initial overburden pressure

u = pore water pressure

Δu_r = residual pore water pressure

APPENDIX III. TABLES

Table 1: Summary of Model Test Data for Centrifuge Tests GF3-GF6 and SL1-SL2

Test	Description	Base Motion	Nevada Sand		Silica Flour	
			e_o	γ_b (pcf)	e_o	γ_b (pcf)
GF3	Silt on sand (edge effects)	Sine	0.67	62.9	0.85	55.7
GF4	Silt on a mound of level sand	Sine	0.67	62.9	0.84	56.0
GF5	Silt on a mound of sloped sand	E.C.	0.67	62.9	0.80	57.2
GF6	Silt on a mound of sloped sand	E.C.	0.67	62.9	0.74	59.2
SL1	Uniform sand level, dry	E.C.	0.67	62.9	----	----
SL2	Uniform sand, level, wet	E.C.	0.67	62.9	----	----

APPENDIX III. TABLES (CONT.)

Table 2: Description of Soils

Soil Type	D_{50} (mm)	e_{max}	e_{min}	k (cm/s)
Base Sand	0.40	0.851	0.557	----
Nevada Sand	0.13	0.894	0.516	3×10^{-3}
Silt (Silica Flour)	----	----	----	3×10^{-6}

Table 3: Centrifuge Scaling Laws

Quantity	Full Scale (prototype)	Centrifuge Model @ Ng
Length (l)	1	1/N
Acceleration (a)	1	N
Frequency (f)	1	N
Time (t)	1	1/N
Permeability (k)	1	1/N

APPENDIX IV. FIGURES

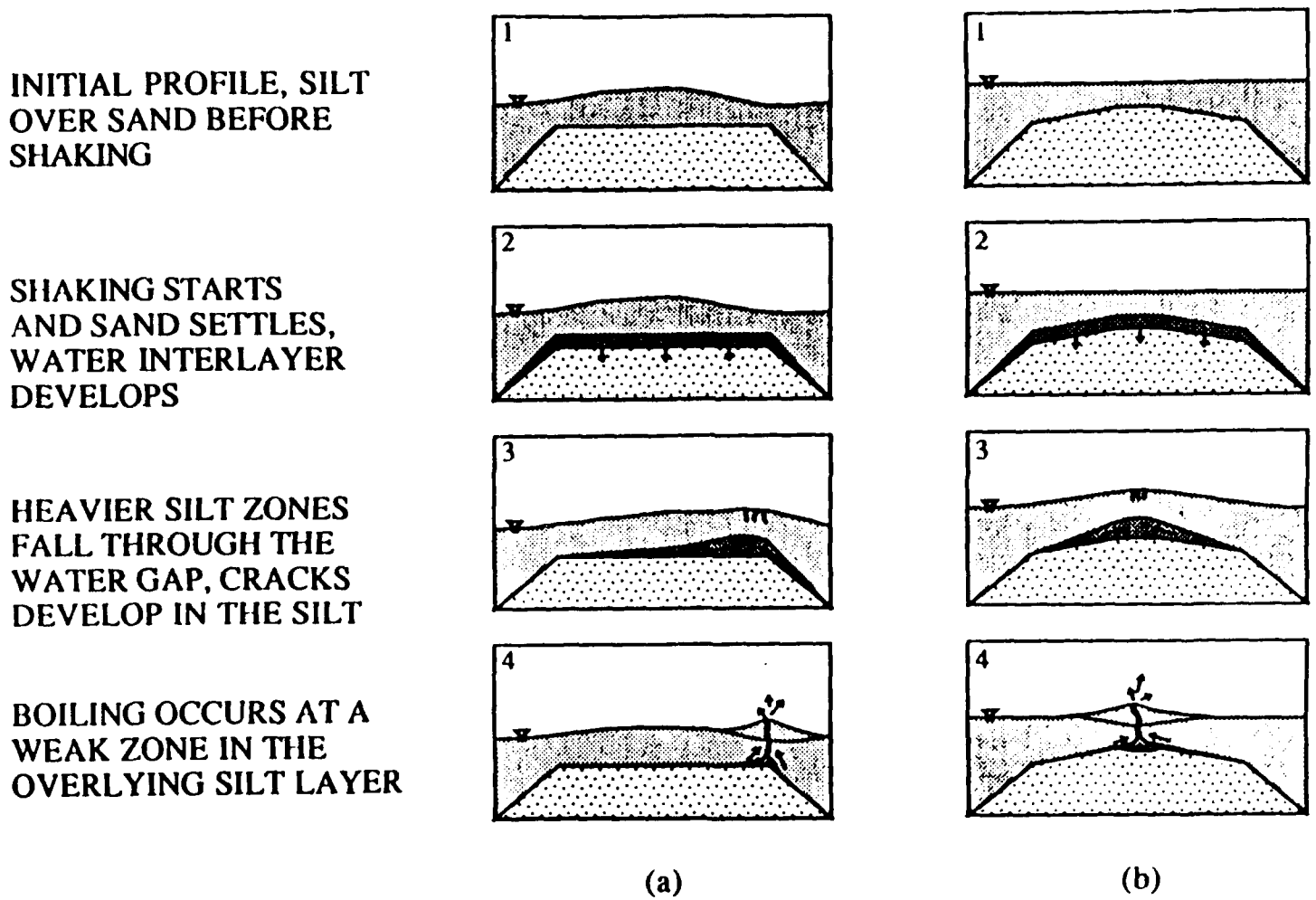

Figure 1: The mechanism of liquefaction in layered soils as observed in centrifuge model tests: (a) a sloping surface and a level interface leads to a thin zone at the right side of the model, test GF4, and (b) a level surface with a sloping interface leads to a thin zone at the center of the model, tests GF5 and GF6.

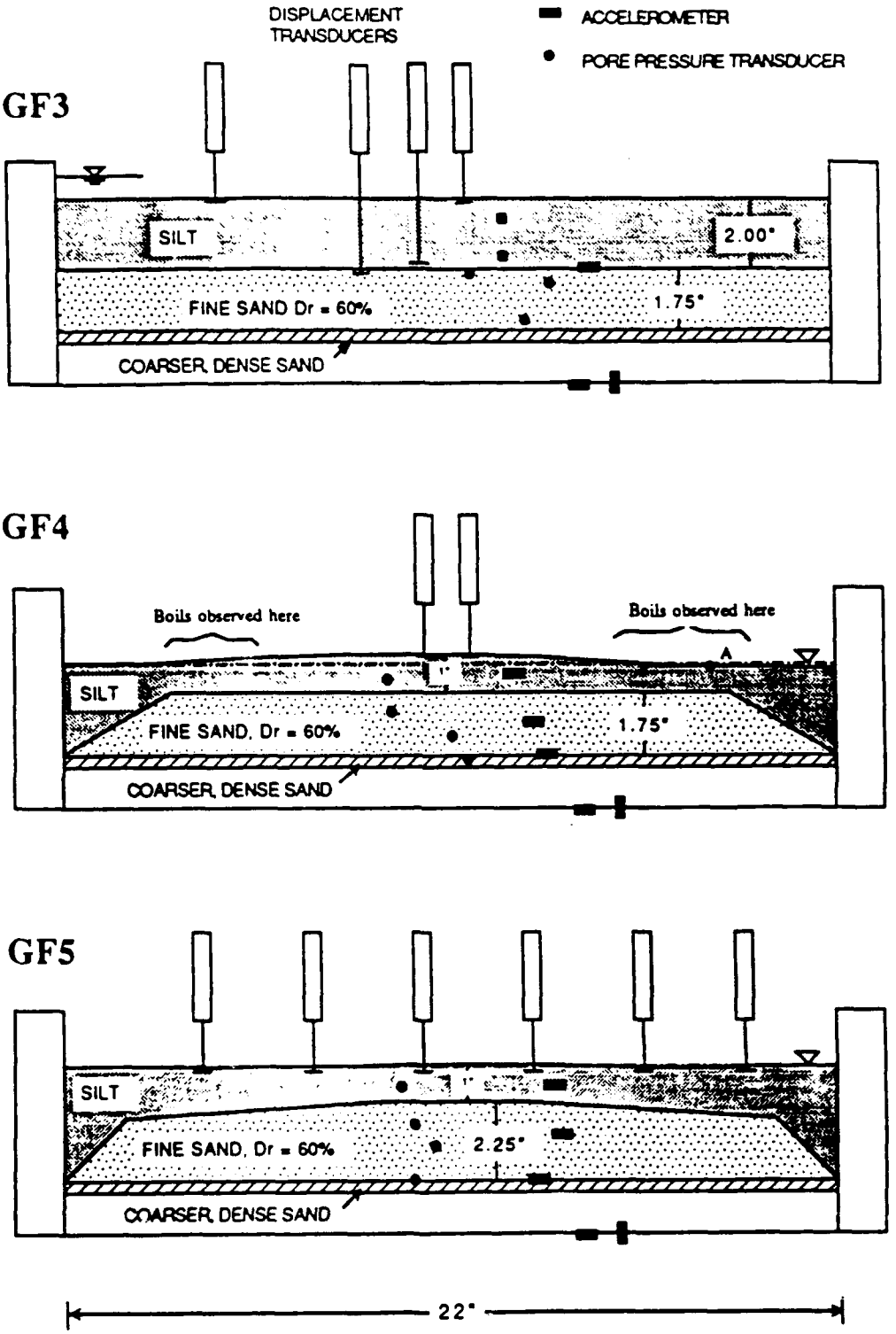

Figure 2: Centrifuge model test configurations: (a) model test GF3, (b) model test GF4, and (c) model test GF5.

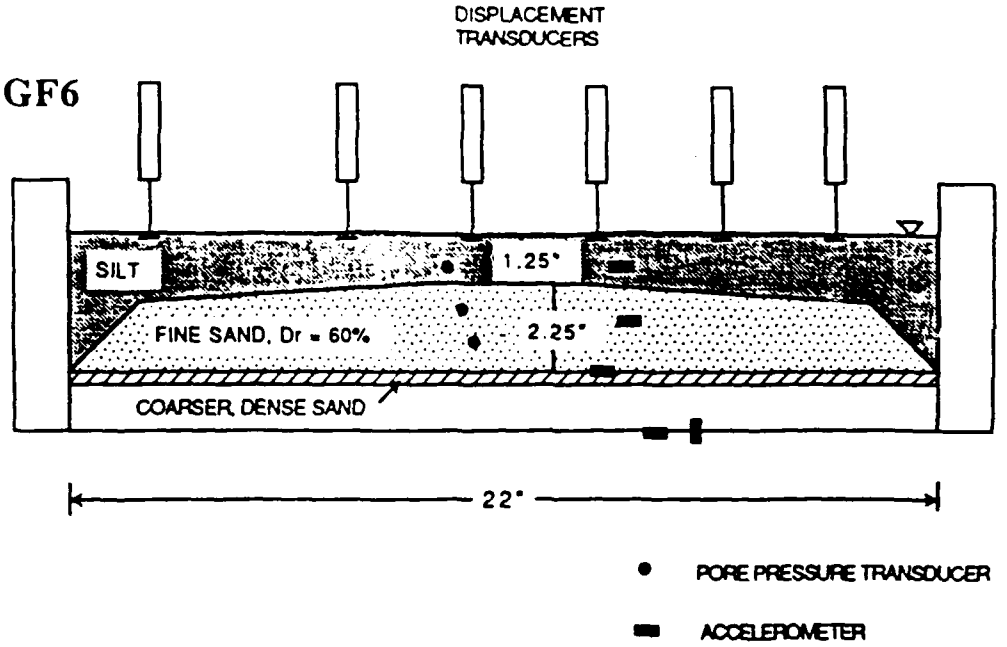

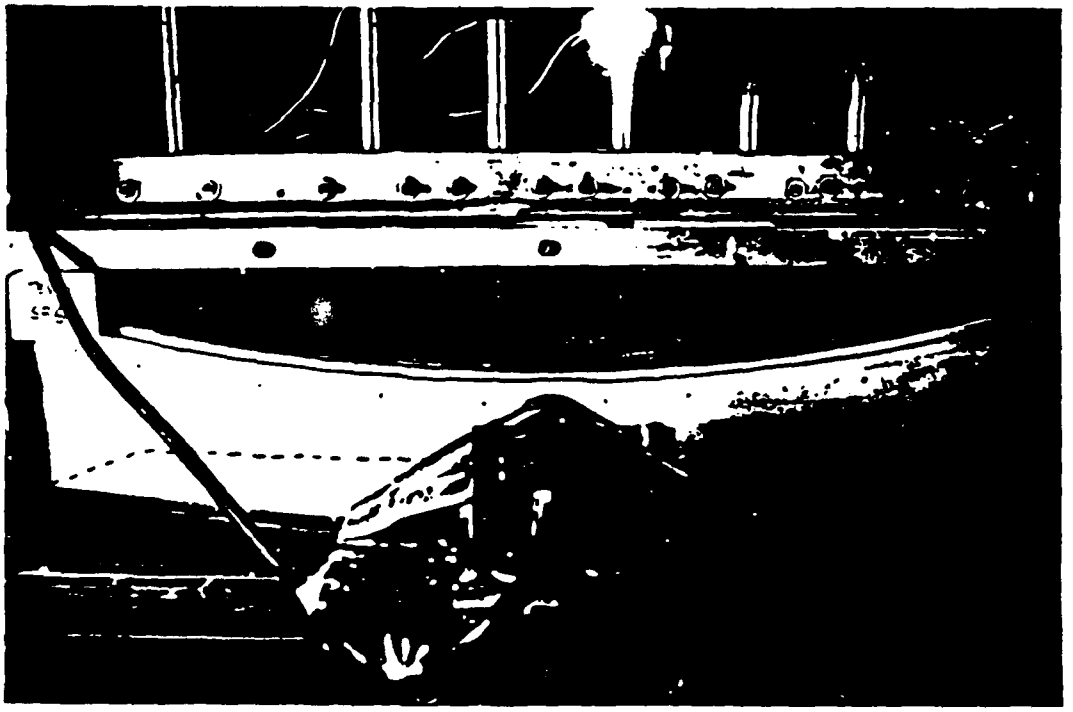

Figure 3: The model test configuration used for centrifuge test GF6: (a) a sketch of the model, and (b) a photograph of the model prior to shaking.

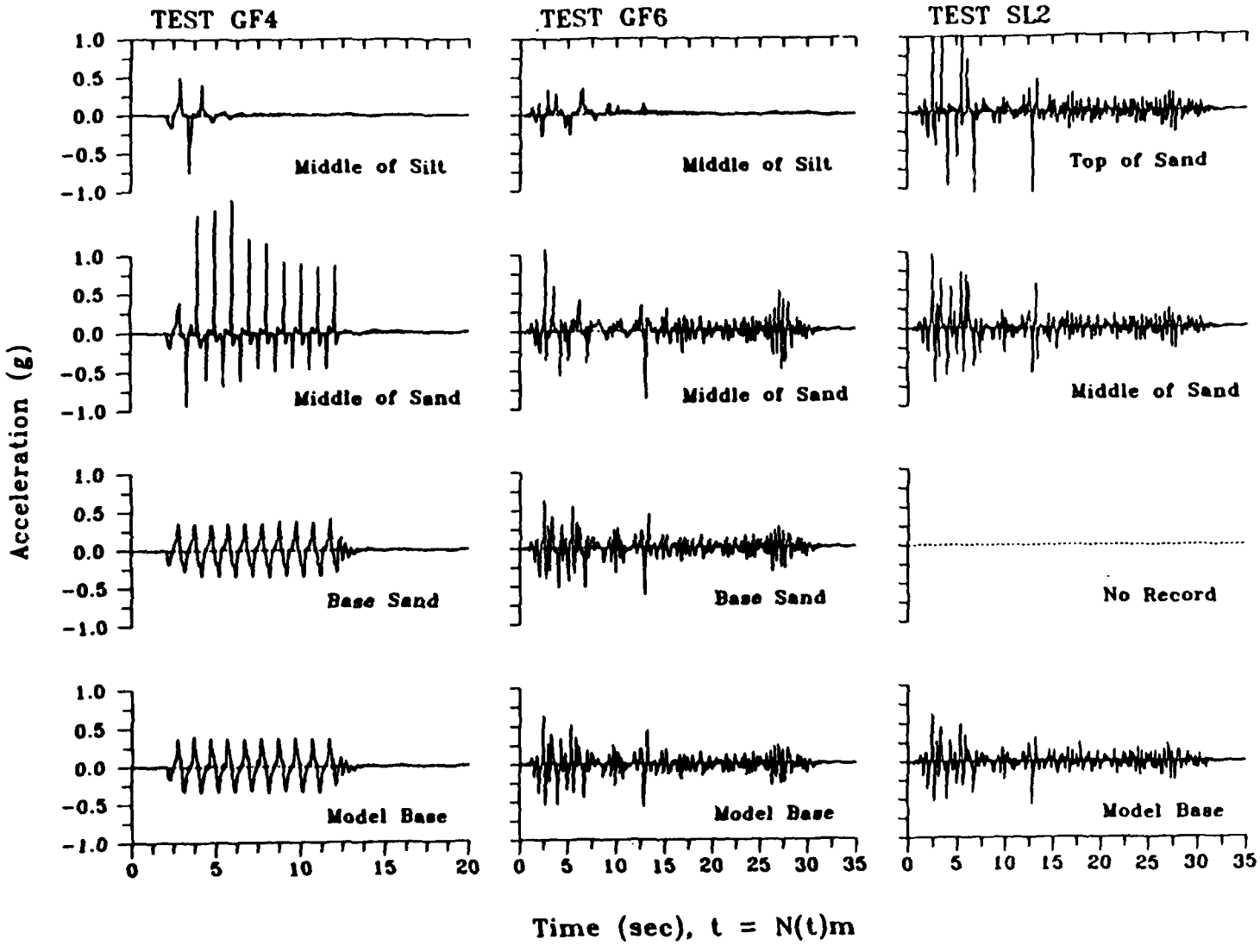

Figure 4: Horizontal acceleration time histories recorded for tests GF4, GF6, and SL2. Transducer locations are noted below each trace; data is presented in prototype terms.

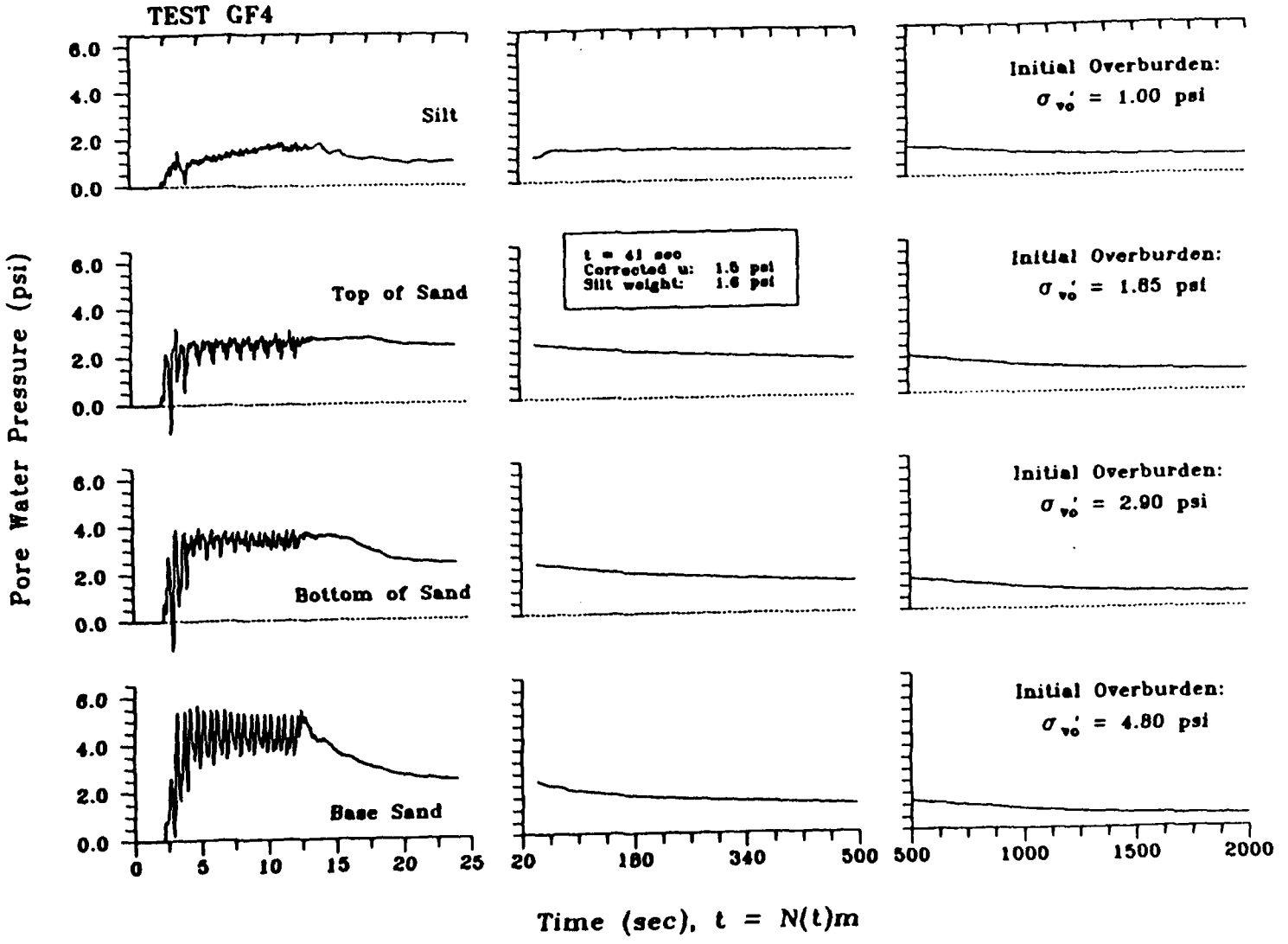

Figure 5: Pore water pressure time histories recorded for test GF4. Transducer locations are noted; data is presented in prototype terms with pressure expressed in psi. Note that three different time scales are used.

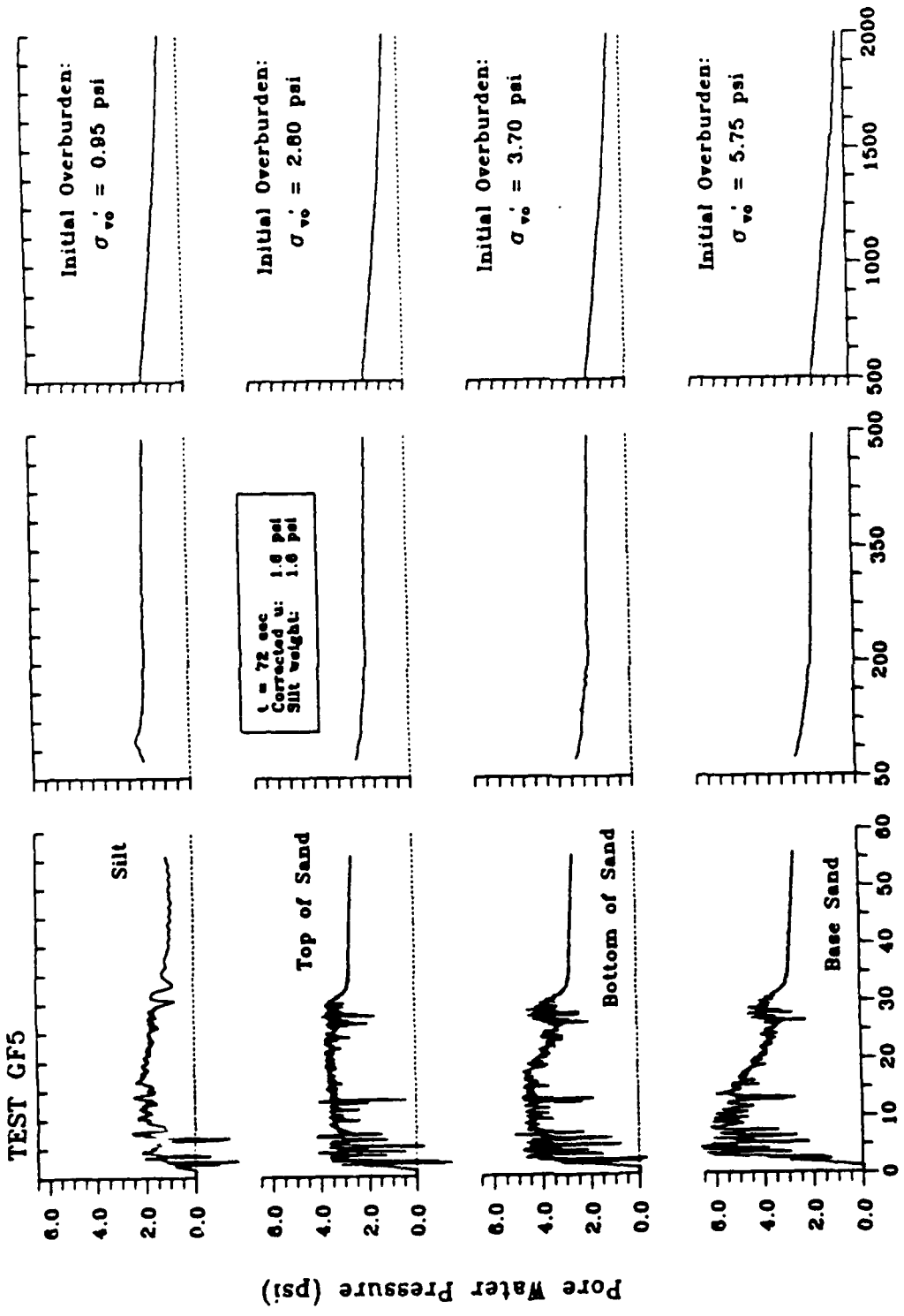

Figure 6: Pore water pressure time histories recorded for test GF5. Transducer locations are noted; data is presented in prototype terms with pressure expressed in psi. Note that three different time scales are used.

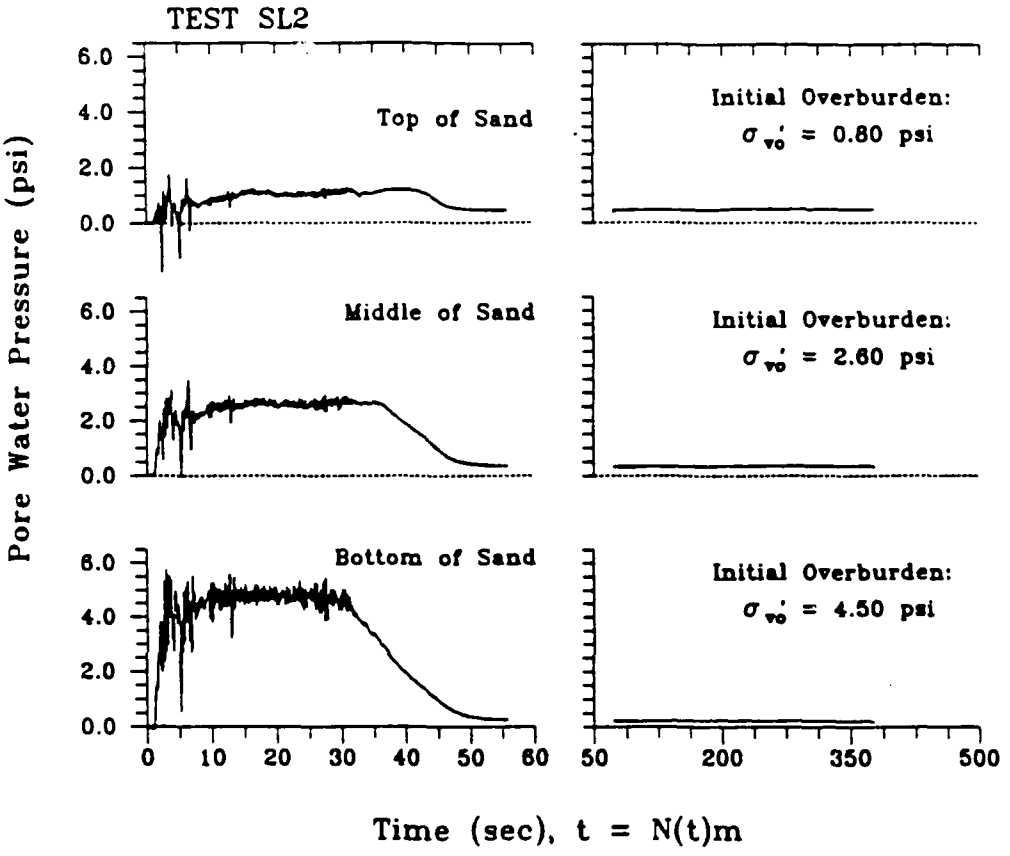

Figure 7: Pore water pressure time histories recorded for test SL2. Transducer locations are noted; data is presented in prototype terms with pressure expressed in psi. Note that two different time scales are used.

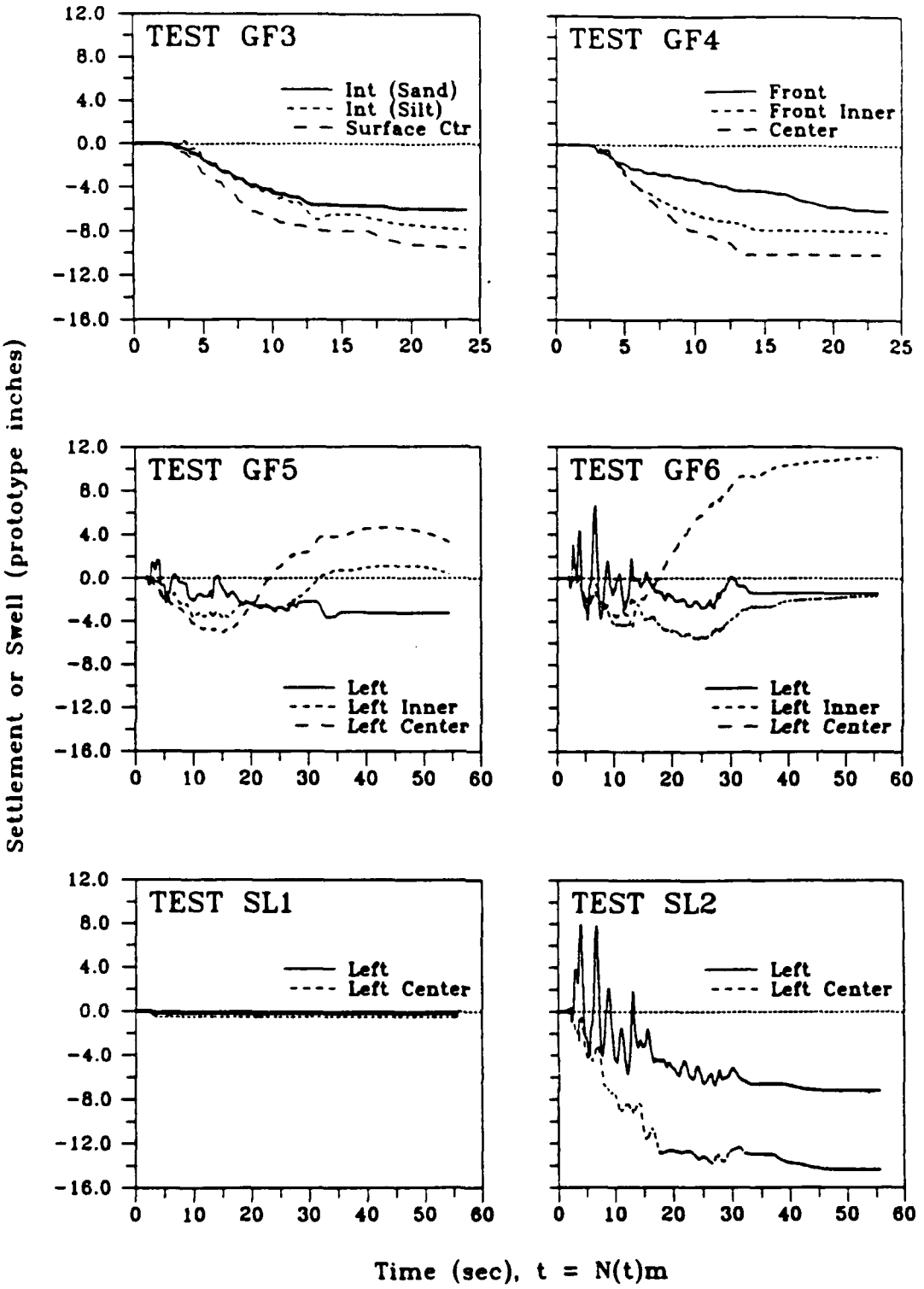

Figure 8: Settlement time histories recorded during tests GF3, GF4, GF5, GF6, SL1, and SL2. Settlement (or swell) is expressed in prototype inches. Displacement transducer locations are noted in each plot.

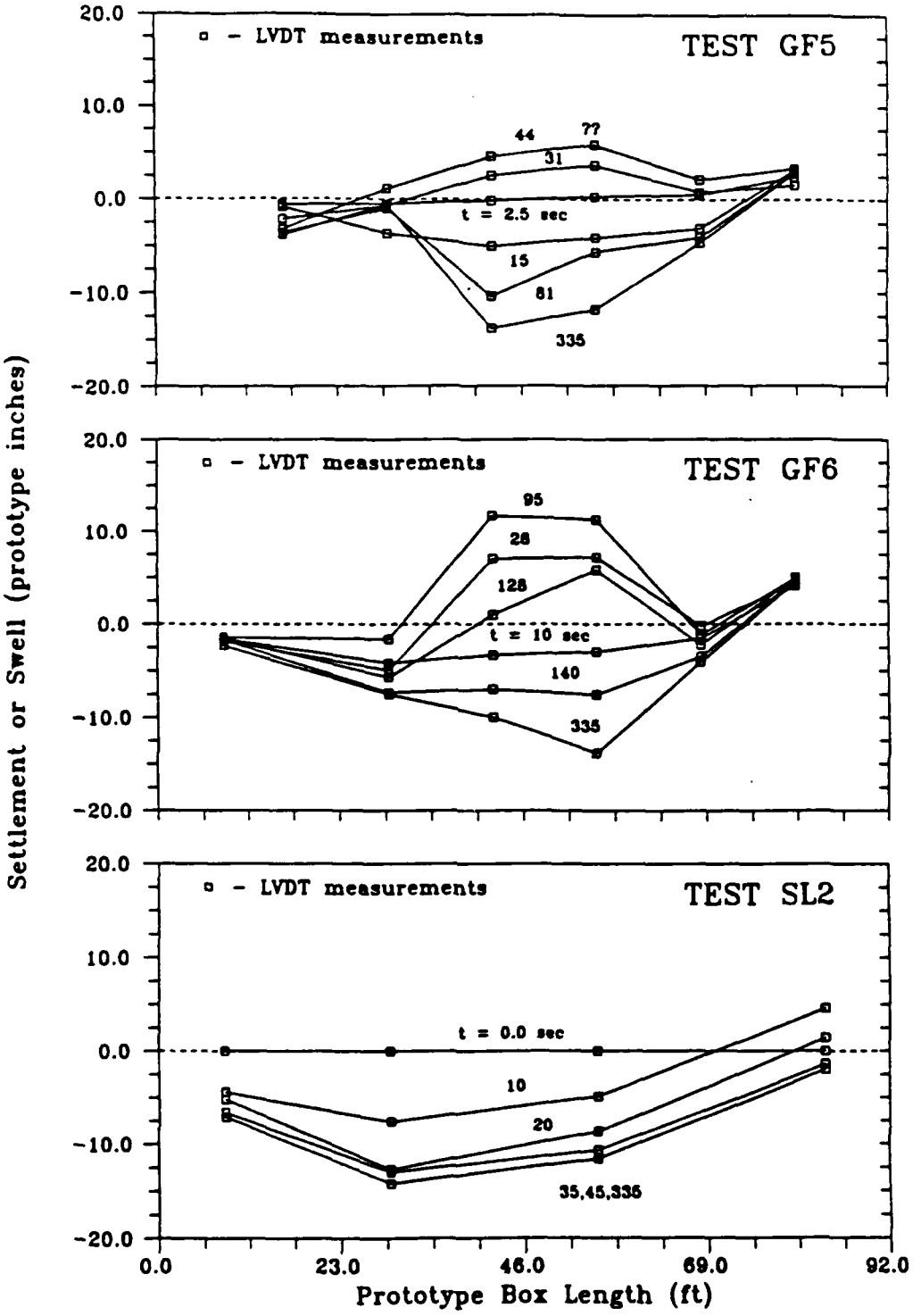

Figure 9: Surface profiles observed for tests GF5, GF6, and SL2. Settlement (or swell) is expressed in prototype inches along the vertical axis while the model box length is expressed in prototype feet along the horizontal axis. Time, $t = N(t)_m$, on each plot denotes the time after shaking at which the profile was measured.

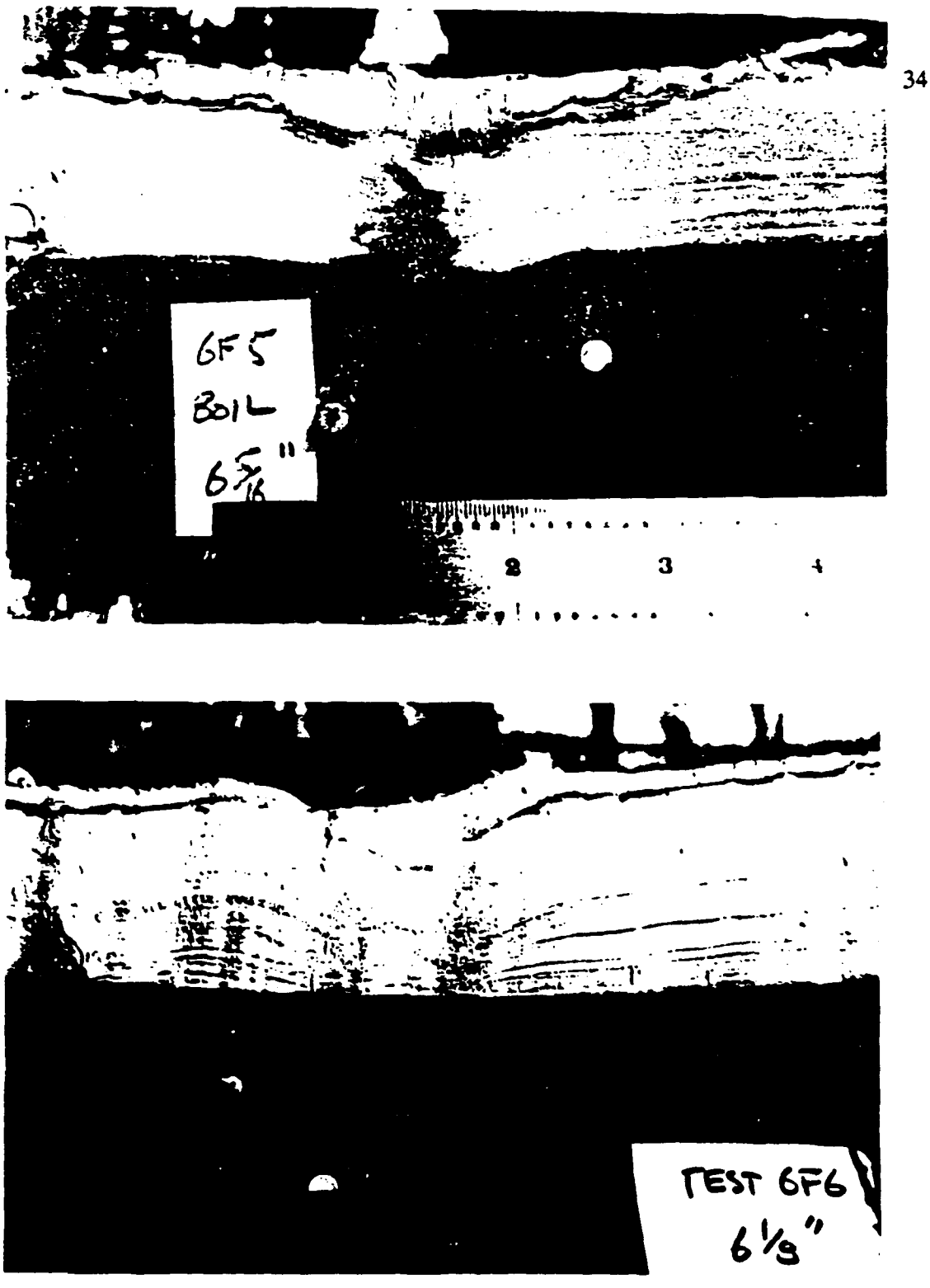

Figure 10: Photographed cross-sections for tests GF5 and GF6 showing the boiling that occurred at the center of the model. Inch measurements in the photographs denote the distance from the front of the model box.

DISTRIBUTION LIST

ADINA ENGRG, INC / WALCZAK, WATERTOWN, MA
AFOSR / NA (WU), WASHINGTON, DC
APPLIED RSCH ASSOC, INC / HIGGINS, ALBUQUERQUE, NM
APTEK / SCHWER, SAN JOSE, CA
ARMSTRONG AERO MED RSCH LAB / OVENSHIRE, WRIGHT PATTERSON AFB, OH
ARMY CORPS OF ENGRS / HQ, DAEN-ECE-D, WASHINGTON, DC
ARMY EWES / FRANKLIN, VICKSBURG, MI
ARMY EWES / WES (NORMAN), VICKSBURG, MS
ARMY EWES / WES (PETERS), VICKSBURG, MS
ARMY EWES / WESIM-C (N. RADHAKRISHNAN), VICKSBURG, MS
BUREAU OF RECLAMATION / MCLEAN, DENVER, CO
CAL TECH / HUSHMAND, PASADENA, CA
CAL TECH / SCOTT, PASADENA, CA
CATHOLIC UNIV / CE DEPT (KIM) WASHINGTON, DC
CENTRIC ENGINEERING SYSTEMS INC / TAYLOR, PALO ALTO, CA
DOT / TRANSP SYS CEN (TONG), CAMBRIDGE, MA
DTIC / ALEXANDRIA, VA
DTRCEN / (CODE 1720), BETHESDA, MD
EARTH TECH / MURALEETHARAN, IRVINE, CA
GEN MOTORS RSCH LABS / (KHALIL), WARREN, MI
GEORGIA TECH / CHAMEAU, ATLANTA, GA
GEORGIA TECH / MECH ENGRG (FULTON), ATLANTA, GA
HKS INC / LOOP NAGTEGAAL PROVIDENCE, RI
HQ AFESC / RDC (DR. M. KATONA), TYNDALL AFB, FL
LAWRENCE LIVERMORE NATIONAL LAB / WHIRLEY, LOVERMORE, CA
LOCKHEED / RSCH LAB (M. JACOBY), PALO ALTO, CA
LOCKHEED / RSCH LAB (P UNDERWOOD), PALO ALTO, CA
MARC ANALYSIS RSCH CORP / HSU, PALO ALTO, CA
MEDWADOWSKI, S. J. / CONSULT STRUCT ENGR, SAN FRANCISCO, CA
MIT / WHITMAN, CAMBRIDGE, MA
NAVFACENGCOM / CODE 04B2 (J. CECILIO), ALEXANDRIA, VA
NAVF[illegible]ENGCOM / CODE 04BE (WU), ALEXANDRIA, VA
NOR[illegible]STERN UNIVERSITY / BAZANT, EVANSTON, IL
NORTHWESTERN UNIVERSITY / CE DEPT (BELYTSCHKO), EVANSTON, IL
NRL / CODE 4430, WASHINGTON, DC
NSF / STRUC & BLDG SYSTEMS (KP CHONG), WASHINGTON, DC
NUSC DET / CODE 44 (CARLSEN), NEW LONDON, CT
OCNR / CODE 10P4 (KOSTOFF), ARLINGTON, VA
OCNR / CODE 1121 (EA SILVA), ARLINGTON, VA
OHIO STATE UNIVERSITY / CE DEPT (SIERAKOWSKI), COLUMBUS, OH
OHIO STATE UNIVERSITY / WU, COLUMBUS, OH
ONR / CODE 1131S, ARLINGTON, VA
ONR / CODE 1132SM, ARLINGTON, VA
OREGON STATE UNIV / CE DEPT (HUDSPETH), CORVALLIS, OR
OREGON STATE UNIV / CE DEPT (LEONARD), STORRS, CT
OREGON STATE UNIV / CE DEPT (YIM), CORVALLIS, OR
OREGON STATE UNIV / DEPT OF MECH ENGRG (SMITH), CORVALLIS, OR

PORT OF LA / LEE, SAN PEDRO, CA
PORT OF LA / WITTKOP, SAN PEDRO, CA
PORTLAND STATE UNIV / ENGRG DEPT (MIGLIORI), PORTLAND, OR
PRINCETON UNIV / PREVOST, PRINCETON, NJ
SCOPUS TECHNOLOGY INC / (B NOUR-OMID), EMERYVILLE, CA
SCOPUS TECHNOLOGY INC / (S. NOUR-OMID), EMERYVILLE, CA
SRI INTL / ENGRG MECH DEPT (GRANT), MENLO PARK, CA
SRI INTL / ENGRG MECH DEPT (SIMONS), MENLO PARK, CA
STANFORD UNIV / APP MECH DIV (HUGHES), STANFORD, CA
STANFORD UNIV / CE DEPT (PENSKY), STANFORD, CA
STANFORD UNIV / DIV OF APP MECH (SIMO), STANFORD, CA
STANFORD UNIV / KIREMIDJIAM, STANFORD, CA
TRW INC / CRAWFORD, REDONDO BEACH, CA
TUFTS UNIV / SANAYEI, MEDFORD, MA
UNIV OF CALIFORNIA / CE DEPT (HERRMANN), DAVIS, CA
UNIV OF CALIFORNIA / CE DEPT (KUTTER), DAVIS, CA
UNIV OF CALIFORNIA / CE DEPT (RAMEY), DAVIS, CA
UNIV OF CALIFORNIA / CE DEPT (ROMSTAD), DAVIS, CA
UNIV OF CALIFORNIA / CTR FOR GEOTECH MODEL (IDRISS), DAVIS, CA
UNIV OF CALIFORNIA / FOURNEY, LOS ANGELES, CA
UNIV OF CALIFORNIA / MECH ENGRG DEPT (BAYO), SANTA BARBARA, CA
UNIV OF CALIFORNIA / MECH ENGRG DEPT (BRUCH), SANTA BARBARA, CA
UNIV OF CALIFORNIA / MECH ENGRG DEPT (LECKIE), SANTA BARBARA, CA
UNIV OF CALIFORNIA / MECH ENGRG DEPT (MCMEEKING), SANTA BARBARA, CA
UNIV OF CALIFORNIA / MECH ENGRG DEPT (MITCHELL), SANTA BARBARA, CA
UNIV OF CALIFORNIA / MECH ENGRG DEPT (TULIN), SANTA BARBARA, CA
UNIV OF CALIFORNIA / SEED, BERKELEY, CA
UNIV OF CALIFORNIA / SELMA, LOS ANGELES, CA
UNIV OF CALIFORNIA / WILSON, BERKELEY, CA
UNIV OF COLORADO / CE DEPT (HON-YIM KO), BOULDER, CO
UNIV OF COLORADO / MECH ENGRG DEPT (FELLIPA), BOULDER, CO
UNIV OF COLORADO / MECH ENGRG DEPT (PARK), BOULDER, CO
UNIV OF COLORADO / STURE, BOULDER, CO
UNIV OF ILLINOIS / CE LAB (ABRAMS), URBANA, IL
UNIV OF ILLINOIS / CE LAB (PECKNOLD), URBANA, IL
UNIV OF ILLINOIS / GHABOUSSI, URBANA, IL
UNIV OF N CAROLINA / CE DEPT (GUPTA), RALEIGH, NC
UNIV OF N CAROLINA / CE DEPT (TUNG), RALEIGH, NC
UNIV OF NEVADA / SIDDHARTAN, RENO, NV
UNIV OF SOUTHERN CALIFORNIA / JEAN-PIERRE BARDET, LOS ANGELES, CA
UNIV OF TEXAS / CE DEPT (STOKOE), AUSTIN, TX
UNIV OF TEXAS / ROESSET, AUSTIN, TX
UNIV OF WYOMING / CIVIL ENGRG DEPT, LARAMIE, WY
US COE / WALZ, WASHINGTON, DC
WEBSTER, R / BRIGHAM CITY, UT
WEIDLINGER ASSOC / F.S. WONG, LOS ALTOS, CA
WOODWARD CLYDE CONSULTANTS / MORIWAKI, SANTA ANA, CA